J|A|C|S
ARTICLES
Published on Web 04/26/2006

Effect of Hydration on Coordination Properties of Uranyl(VI) Complexes. A First-Principles Molecular Dynamics Study

Michael Bühl,*,† Hendrik Kabrede,† Romain Diss,‡ and Georges Wipff‡

Contribution from the Max-Planck-Institut für Kohlenforschung, Kaiser-Wilhelm-Platz 1, D-45470 Mülheim an der Ruhr, Germany, and UMR 7177 CNRS, Laboratoire MSM, Institut de Chimie, 4 rue Blaise Pascal, 67000 Strasbourg, France

Received October 26, 2005; E-mail: buehl@mpi-muelheim.mpg.de

Abstract: Results from Car−Parrinello molecular dynamics simulations are reported for $[UO_2(OH_2)_5]^{2+}$, $UO_2(NO_3)_2(OH_2)_2$, and $UO_2(NO_3)_2(\eta^2$-tmma) (tmma = tetramethylmalonamide) in the gas phase and in aqueous solution. The distances between uranyl and neutral ligands such as water and tmma are decreased by up to 0.2 Å upon hydration, whereas those between uranyl and the nitrate ion are increased by up to 0.08 Å. According to pointwise thermodynamic integration involving constrained molecular dynamics simulations, solvation facilitates the transition of the chelating nitrate ligand to a η^1-bonding mode: the free energy of $UO_2(\eta^2$-$NO_3)(\eta^1$-$NO_3)(OH_2)_2$ relative to the bis-chelating minimum drops from 3.9 kcal/mol in vacuo to 1.4 kcal/mol in water. Optimizations in a polarizable continuum (specifically, the conductor-like screening model in conjunction with the zero-order regular approximation and triple-ζ Slater basis sets) can qualitatively reproduce the geometrical changes from explicit hydration.

Introduction

The quest for ever more stable and extractable uranyl(VI) complexes is the holy grail of nuclear-waste reprocessing. The goal is to design scavenger ligands that bind selectively and with high affinity to uranyl present in spent nuclear fuel after dissolution in aqueous nitric acid,[1,2] or present in the human body after uranium poisoning.[3] Many of these ligands are bi- or polydentate in nature, exploiting the well-known chelate effect.[4] For lanthanide and actinide complexes, the precise magnitude of this effect, as well as its origin, is not yet fully understood. The common explanation in terms of entropy gain after displacement of two monodentate ligands with a bidentate one is only one aspect,[5] as the enthalpic contributions to the binding can depend strongly on factors such as steric crowding, ring size, or hardness of the cation.[6] In fact, quantum-chemical calculations at Hartree−Fock and DFT levels have indicated that, in the gas phase, typical chelating ligands such as malonamides and succinamides bind less strongly in bidentate fashion to uranyl than two corresponding monodentate analogues, with enthalpic differences up to 24 kcal/mol (B3LYP) in favor of the latter.[6b]

Even for the nitrate anion, which in the vast majority of cases binds in η^2-mode via two oxygen atoms to transition metals, η^1-coordination can, according to B3LYP calculations for microsolvated clusters, become competitive for lanthanide ions.[7,8] What emerged from these studies is that it is not only essential to have the first coordination sphere of the metal saturated in order to obtain meaningful energetics but that water molecules formally belonging to the second solvation shell can also have a noticeable impact on structures and energies. In such a situation, static optimizations of realistically large clusters are a formidable task due to the myriads of local minima that can be involved. Molecular dynamics (MD) simulations of the actual solution are an obvious way around this problem, since they are, after proper equilibration, free of any bias due to a particular choice of the initial configuration. Classical MD simulations using molecular mechanical (MM) force fields are well established for the study of uranyl complexes in various solvents and interfaces.[9] MD studies on potential energy surfaces derived from quantum mechanics (QM) are an attractive bridge between both worlds (static QM and classical MD calculations) but are yet very scarce for actinides.

† Max-Planck-Institut für Kohlenforschung.
‡ Laboratoire MSM.

(1) McKibben, J. M. *Radiochim. Acta* **1984**, *36*, 3−15.
(2) Paiva, A. P.; Malik, P. *J. Radioanal. Nucl. Chem.* **2004**, *261*, 485−496.
(3) Gorden, A. E. V.; Xu, J. D.; Raymond, K. N.; Durbin P. *Chem. Rev.* **2003**, *103*, 4207−4282.
(4) See for instance: (a) Sawicki, M.; Siaugue, J.-M.; Jacopin, C.; Moulin, C.; Bailly, T.; Burgada, R.; Meunier, S.; Baret, P.; Pierre, J.-L.; Taran, S. *Chem. Eur. J.* **2005**, *11*, 3689−3697. (b) Jain, V. K.; Pillai, S. G.; Pandya, R. A.; Agrawal, Y. K.; Shrivastav, P. S. *Talanta* **2005**, *65*, 466−475 and references therein.
(5) Vallet, V.; Wahlgren, U.; Grenthe, I. *J. Am. Chem. Soc.* **2003**, *125*, 14941−14950. Choppin, G. *J. Alloys Compd.* **1997**, *249*, 1−18. Hancock, R. D. *J. Chem. Educ.* **1992**, *69*, 615−621. Mathur, J. N.; Murali, M. S.; Nash, K. L. *Solvent Extr. Ion Exch.* **2002**, *19*, 357−390.
(6) (a) Coupez, B.; Boehme, C.; Wipff, G. Phys. *Chem. Chem. Phys.* **2002**, *4*, 5716−5729. (b) Coupez, B.; Wipff, G. *Inorg. Chem.* **2003**, *42*, 3693−3703.
(7) Dobler, M.; Guilbaud, P.; Dedieu, A.; Wipff, G. *New J. Chem.* **2001**, *25*, 1458−1465.
(8) There is also experimental precedence for such a binding mode in the solid, e.g.: (a) Er(terpy)$(NO_3)_3$(EtOH): Cotton, S. A.; Raithby, P. R. *Inorg. Chem. Commun.* **1999**, *2*, 86−88. (b) $La(Ph_3PO)_4(NO_3)_3\cdot Me_2CO$: Levason, W.; Newman, E. H.; Webster, M. *Polyhedron* **2000**, *19*, 2697−2705.
(9) (a) Guilbaud, P.; Wipff, G. *THEOCHEM* **1996**, *366*, 55−63. For more recent examples, see: (b) Baaden, M.; Schurhammer, R.; Wipff, G. *J. Phys. Chem. B* **2002**, *106*, 434−441. (c) Chaumont, A.; Engler, E.; Wipff, G. *Inorg. Chem.* **2003**, *42*, 5348−5356. (d) Chaumont, A.; Wipff, G. *Chem.−Eur. J.* **2004**, *10*, 3919−3930. (e) Galand, N.; Wipff, G. *J. Phys. Chem. B* **2005**, *109*, 277−287.

Chart 1

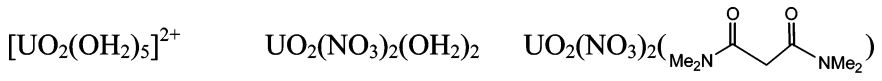

1 **2** **3**

Using a combined QM/MM approach, Infante and Visscher have studied the dynamics of $[UO_2F_4]^{2-}$ in aqueous solution.[10] We have recently communicated results from all-QM Car−Parrinello (CPMD) simulations for aqueous uranyl hydrate, $[UO_2(OH_2)_5]^{2+}$ (**1**), emphasizing the thermodynamic driving force for moving one water ligand from the first to the second solvation shell, or vice versa.[11] We now present a deeper analysis of the CPMD results for **1** than was possible in these communications and extend these studies to a prototypical uranyl nitrate complex, $UO_2(NO_3)_2(OH_2)_2$ (**2**). This species is well characterized by X-ray crystallography[12] and is a good model for the speciation of uranyl(VI) in nitric acid. Special attention is called to the question of η^2- vs η^1-coordination of one of the nitrate ligands and to the role that the surrounding solvent plays in this simple chelate effect. Finally, we include a complex with a typical scavenger ligand, $UO_2(NO_3)_2$(tmma) (**3**) (tmma = tetramethylmalonamide, see Chart 1), which has also been characterized by X-ray crystallography.[13] Taken together, complexes **1**−**3** are models for key species involved in the extraction of uranyl during reprocessing of nuclear waste, and an improved understanding of their structures and dynamics in solution could open ways for better control of this process. Moreover, deeper insights into this kind of uranyl solution chemistry could also further our general understanding of the solubility of uranyl in natural systems, for instance in contaminated water, waste storage tanks, and the evolution of nuclear waste in a geological repository, to name but a few examples.

Further validation of the uranium pseudopotential employed in the CPMD calculations provides additional impetus for the present study. To this end, the results of static geometry optimizations obtained with this computational setup are compared to data produced with other, well-established effective core potentials (ECPs)[14] or an explicit relativistic method using the zero-order regular approximation (ZORA).[15]

Computational Details

Geometries were optimized using the BLYP functional,[16] in conjunction with a variety of computational approaches: LANL denotes calculations performed with the Gaussian 03 program[17] employing the Los Alamos relativistic effective core potential for U together with its (3s3p2d2f) valence basis of contracted Gaussians,[14] standard 6-31G-(d) basis for all other elements, and a medium-sized integration grid (75 radial shells with 302 angular points per shell).

ZORA[18] stands for scalar relativistic calculations using the approximation with the same name (zeroth-order relativistic approximation), a polarized triple-ζ basis of Slater functions for all elements, and a dense integration grid (ACCINT parameter equal to 6). The frozen-core approach was used.[19] Additional optimizations, labeled ZORA(*aq*), were performed in a polarizable continuum employing the COSMO variant,[20] the parameters of water, and a molecule-shaped cavity (defined as solvent-excluding surface with solvent radius of 1.4 Å and the following atomic radii in Å: U 1.86, Cl 1.75, O 1.52, N 1.55, C 1.70, H 1.20). All ZORA computations were performed with the ADF program package.[21]

CP-opt denotes geometries optimized using the density-functional based Car−Parrinello scheme[22] as implemented in the CPMD program,[23] until the maximum gradient was less than 5×10^{-4} au. Norm-conserving pseudopotentials were used that had been generated according to the Troullier and Martins procedure[24] and transformed into the Kleinman−Bylander form.[25] For uranium, the semicore (or small-core) pseudopotential was employed that had been generated and validated in ref 11a. Periodic boundary conditions were imposed using cubic or orthorhombic supercells adjusted to the size of the complexes ($13 \times 13 \times 13$ Å^3 for **1**, both $13 \times 13 \times 13$ and $16 \times 13 \times 16$ Å^3 for **2**, and $19 \times 16 \times 12$ Å^3 for **3**−**6**). Kohn−Sham orbitals were expanded in plane waves at the Γ-point up to a kinetic energy cutoff of 80 Ry. For the complexes in vacuo, Car−Parrinello molecular dynamics simulations (denoted CPMD) were performed in the NVT ensemble using a single Nosé−Hoover thermostat set to 300 K (instantaneous heat-up, frequency 1800 cm^{-1}), a fictitious electronic mass of 600 au, and a time step of 0.121 fs. These unconstrained simulations were followed over 2−10 ps, the first 0.5 ps of which was taken for equilibration. For the aqueous solutions, labeled CPMD(*aq*), the boxes were filled with 58, 100, and 107 water molecules for **2** in the smaller box, **2** in the larger box, and **3**, respectively, so that the density of the resulting solutions, 1.11, corresponds to that of typical uranyl complexes (e.g., uranyl nitrate) with the same concentration, 16 wt %.[26] To increase the time step, hydrogen was substituted with deuterium. Long-range electrostatic interactions were treated with the Ewald method. No electrostatic decoupling between replicated cells was included, as it had been shown that no noticeable errors are introduced by this

(10) Infante, I.; Visscher, L. *J. Comput. Chem.* **2003**, *25*, 386-392.
(11) (a) Bühl, M.; Diss, R.; Wipff, G. *J. Am. Chem. Soc.*, **2005**, *127*, 13506−13507. (b) Bühl, M.; Kabrede, H. *Inorg. Chem.*, in press.
(12) A search for the $UO_2(NO_3)_2(OH_2)$ fragment in the Cambridge Structure Database affords 15 hits containing **3**; for the most recent ones, see: (a) Charushnikova, I. A.; Den Auwer, C. *Koord. Khim.* **2004**, *30*, 546−554 (*Russ. J. Coord. Chem.* **2004**, *30*, 511−519, ref-code AZECUD). (b) Villiers, C.; Thuery, P.; Ephritikhine, M. *Polyhedron* **2004**, *23*, 1613−1618 (ref-codes AZOTAK and AZOTEO).
(13) (a) Lumetta, G. J.; McNamara, B. K.; Rapko, B. M.; Sell, R. L.; Rogers, R. D.; Broker, G.; Hutchison, J. E. *Inorg. Chim. Acta* **2000**, *309*, 103−108. (b) For the X-ray structure of the succinamide analogue of **4a**, see: Wang, H.-Z.; Cui, L.; Cao, Z.-B.; Gu, J.-S.; Zhu, L.-M. *Acta Chim. Sin. (Chinese Edition)* **1993**, *51*, 880−884.
(14) Ortiz, J. V.; Hay, P. J.; Martin, R. L. *J. Am. Chem. Soc.* **1992**, *114*, 2736−2737 and references therein.
(15) Wolff, S. K.; Ziegler, T.; van Lenthe, E.; Baerends, E. J. *J. Chem. Phys.* **1999**, *110*, 7689−7698.
(16) (a) Becke, A. D. *Phys. Rev. A* **1988**, *38*, 3098−3100. (b) Lee, C.; Yang, W.; Parr, R. G. *Phys. Rev. B* **1988**, *37*, 785−789.
(17) Frisch, M. J. et al. *Gaussian 03*; Gaussian, Inc.: Pittsburgh, PA, 2003 (see Supporting Information for full citation).
(18) (a) van Lenthe, E.; Baerends, E. J.; Snijders, J. G. *J. Chem. Phys.* **1993**, *99*, 4597−4610. (b) van Lenthe, E.; Baerends, E. J.; Snijders, J. G. *J. Chem. Phys.* **1994**, *101*, 9783−9792. (c) van Lenthe, E.; Ehlers, A. E.; Baerends, E. J. *J. Chem. Phys.* **1999**, *110*, 8943−8953.
(19) The frozen core electrons are the 1s shell for C, O, and N; 1s, 2s, 2p for Cl; and 1s, 2s, 2p, 3s, 3p, 3d, 4s, 4p, 4d, 5s, 5p, 4f, 5d for U.
(20) (a) Pye, C. C.; Ziegler, T. *Theor. Chem. Acc.* **1999**, *101*, 396. (b) Klamt, A.; Schüürmann, G. *J. Chem. Soc., Perkin Trans.* **1993**, *2*, 799−805.
(21) (a) te Velde, G.; Bickelhaupt, F. M.; van Gisbergen, S. J. A.; Fonseca Guerra C.; Baerends, E. J.; Snijders, J. G.; Ziegler, T. *J. Comput. Chem.* **2001**, *22*, 931−967. (b) Fonseca Guerra, C.; Snijders, J. G.; te Velde, G.; Baerends, E. J. *Theor. Chem. Acc.* **1998**, *99*, 391−403. (c) Baerends, E. J. et al. *ADF2004.01, SCM*; Theoretical Chemistry, Vrije Universiteit: Amsterdam, The Netherlands, http://www.scm.com (see Supporting Information for full citation).
(22) Car, R.; Parrinello, M. *Phys. Rev. Lett.* **1985**, *55*, 2471−2474.
(23) *CPMD*, version 3.7.0; Copyright IBM Corp. 1990−2001, Copyright MPI für Festkörperforschung Stuttgart 1997−2001.
(24) Troullier, N.; Martins, J. L. *Phys. Rev. B* **1991**, *43*, 1993−2006.
(25) Kleinman, L.; Bylander, D. M. *Phys. Rev. Lett.* **1982**, *48*, 1425−1428.
(26) For example, see: Lax, E., Ed. *D'Ans-Lax Taschenbuch für Chemiker und Physiker*, 3rd ed.; Springer-Verlag: Berlin, 1967; Vol. 1.

Chart 2

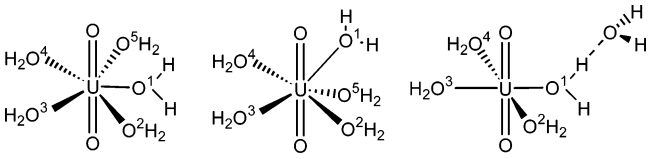

1a **1b** **1c**

procedure even for divalent ions.[27] The CPMD(*aq*) simulations were started from well-equilibrated classical MD runs using the Amber force field.[28]

Atomic charges were obtained from Mulliken (MPA) and Natural Population Analysis (NPA).[29] Wave functions from CPMD snapshots were fully converged for this purpose, and the orbitals represented in plane waves were projected onto suitable atomic orbitals.[30]

Constrained CPMD and CPMD(*aq*) simulations were performed along a predefined reaction coordinate connecting **2a** and **2b** (see section 2 below), to evaluate the change in the Helmholtz free energy by pointwise thermodynamic integration (PTI).[31] The difference Δr between two U−O(nitrate) distances was chosen as a reaction coordinate and was increased successively from zero in steps of 0.2 Å. At each point, the system was propagated until the mean constrained force, $\langle f \rangle$, was sufficiently converged (usually within 1.5−2 ps after 0.5 ps of equilibration, similar to the degree of convergence documented in Figure S1 of the Supporting Information for ref 11a). These simulations were performed in the smaller, cubic box ($13 \times 13 \times 13$ Å^3).

Results and Discussion

1. $[UO_2(OH_2)_5]^{2+}$. In the gas phase, two distinct stationary points were located on the potential energy surface (PES), one with approximate D_5 (**1a**) and one with approximate C_s symmetry (**1b**); see Chart 2. Structure **1a** with planar UOH_2 moieties and with the H atoms essentially aligned along the UO_2 axis is the commonly observed minimum. Structure **1b** has a distinctly nonplanar, envelope-like arrangement of the equatorial O atoms about U. At all levels, **1a** and **1b** are very similar in energy (Table 1), betraying a rather shallow PES as far as the arrangement of the five equatorial water ligands is concerned. In fact, different theoretical methods sometimes arrive at slightly different minima, e.g., with a variable degree of rotation about U−O(H_2) bonds.[32] The tetracoordinated isomer with externally bonded water, $[UO_2(OH_2)_4]^{2+}\cdot H_2O$ **(1c)**, is more stable than **1a** or **1b** by ca. 4−5 kcal/mol (in vacuo). We note that all gas-phase BLYP results in Table 1 are consistent with each other; that is, they afford essentially the same minima with very similar geometrical parameters and relative energies. This mutual accord is reassuring, since, apart from the common functional, quite different types of basis sets and treatments of relativity are involved. It is thus unlikely that a particular choice of the latter would introduce any artifacts.

In a CPMD simulation in the gas phase, **1a** and **1b** interconvert rapidly by way of a pseudorotation-type mechanism, where each of the five water ligands is successively dislocated from the equatorial plane. This fluxional motion causes the ligands to be "smeared out" above and below this plane, as is illustrated in the top of Figure 1, an overlay of ca. 100 snapshots taken during 2.5 ps.

On going from the gas phase into the aqueous solution, the uranyl U═O bonds are slightly elongated, whereas the U−O(H_2) bonds contract noticeably. These trends are both apparent in the CPMD simulations (compare CPMD and CPMD(*aq*) entries in Table 1) as well as in static ZORA optimizations with the COSMO model (compare ZORA and ZORA(*aq*) entries in Table 1). The observation that a polarizable continuum model (PCM) *with a molecule-shaped cavity* can apparently mimic specific solute−solvent interactions is in line with previous results for hydrated metal ions, where application of such a PCM affords metal−ligand bond contractions, whereas multipole-expansion models with a spherical cavity predict elongation of these bonds.[33] That the water ligands are more closely and, thus, more tightly bound to uranyl in aqueous solution than in vacuo is also reflected in their dampened fluxional character in the former medium: compared to the situation in the gas phase, the "out-of-plane fluxionality" is significantly reduced in water, and the ligand O atoms are held more rigidly in the equatorial region (bottom of Figure 1). We note that the solvent-induced shortening of the U−OH_2 bonds leads to a better agreement between the calculated and the experimental distances in aqueous solution (2.41, 2.42, and 2.42 Å, respectively, according to EXAFS,[34] X-ray scattering,[35] and X-ray diffraction[36]) and in the solid state (2.42 Å, on average),[37] but the calculated ones are still ca. 0.06 Å too long. The geometry of the coordinated water molecules is also perturbed by solvation: hydrogen bonding to the solvent molecules causes some lengthening of the (U)O−H bonds (from 0.98 Å in the gas phase to 1.01 Å, on the average, in the case of the $[UO_2(OH_2)_5]^{2+}$ complex).

The relative energies for CPMD and CPMD(*aq*) entries in

(27) Marx, D.; Hutter, J.; Parrinello, M. *Chem. Phys. Lett*. **1995**, *241*, 457−462.

(28) Case, D. A.; Pearlman, D. A.; Caldwell, J. W.; Cheatham, T. E., III; Wang, J.; Ross, W. S.; Simmerling, C. L.; Darden, T. A.; Merz, K. M.; Stanton, R. V.; Cheng, A. L.; Vincent, J. J.; Crowley, M.; Tsui, V.; Gohlke, H.; Radmer, R. J.; Duan, Y.; J. Pitera; Massova, I.; Seibel, G. L.; Singh, U. C.; Weiner, P. K.; Kollman, P. A. *AMBER7*; University of California: San Francisco, CA, 2002. The force field parameters used for the molecular dynamics simulations are from ref 9a.

(29) Reed, A. E.; Curtiss, L. A.; Weinhold, F. *Chem. Rev*. **1988**, *88*, 899−926.

(30) Atomic orbitals were taken from the pseudo wave functions involved in construction of the pseudopotentials, except for hydrogen, where a standard Slater function was used.

(31) Sprik, M.; Ciccotti, G. *J. Chem. Phys*. **1998**, *109*, 7737−7744 and references therein.

(32) For selected studies of **1**, e.g., see: (a) Spencer, S.; Gagliardi, L.; Handy, N. C.; Ioannou, A. G.; Skylaris, C. K.; Willets, A.; Simper, A. M. *J. Phys. Chem. A* **1999**, *103*, 1831−1837. (b) Hay, J. P.; Martin, R. L.; Schreckenbach, G. H. *Phys. Chem. A* **2000**, *104*, 6259−6270. (c) Vallet, V.; Wahlgren, U.; Schimmelpfennig, B.; Szabo, Z.; Grenthe, I. *J. Am. Chem. Soc*. **2001**, *123*, 11999−12008. (d) Tsushima, S.; Yang, T. X.; Suzuki, A. *Chem. Phys. Lett*. **2001**, *334*, 365−373. (e) Clavaguéra-Sarrio, C.; Brenner, V.; Hoyau, S.; Marsden, C. J.; Millié, P.; Dognon, J.-P. *J. Phys. Chem. B* **2003**, *107*, 3051−3060. (f) Moskaleva, L. V.; Krüger, S.; Sporl, A.; Rösch, N. *Inorg. Chem*. **2004**, *43*, 4080−4090. (g) Hagberg, D.; Karlström, G.; Roos, B. O.; Gagliardi, L. *J. Am. Chem. Soc*. **2005**, *127*, 14250−14256. (h) Cao, Z.; Balasubramanian, K. *J. Chem. Phys.* **2005**, *123*, 114309.

(33) See: Martinez, J. M.; Pappalardo, R. R.; Sanchez Marcos, E.; Mennucci, B.; Tomasi, J. *J. Phys. Chem. B* **2002**, *106*, 1118−1123 and references therein.

(34) Allen, P. G.; Bucher, J. J.; Shuh, D. K.; Edelstein, N. M.; Reich, T. *Inorg. Chem*. **1997**, *36*, 4676−4683.

(35) Neuefeind, J.; Soderholm, L.; Skanthakumar, S. *J. Phys. Chem. A* **2004**, *108*, 2733−2739.

(36) Åberg, M.; Ferri, D.; Glaser, J.; Grenthe, I. *Inorg. Chem.* **1983**, *22*, 3986−3989.

(37) (a) For $UO_2[ClO_4]_2\cdot 7H_2O$, see: Alcock, N. W.; Esperas, S. *J. Chem. Soc., Dalton Trans.* **1977**, 893−896. (b) For $3(C_{10}H_{20}O_5)$, $[UO_2(H_2O)_5]^{2+}$, $2(ClO_4^-)$, H_3CCN, H_2O, ref-code FUFVIL and $2(C_{12}H_{24}O_6)$, $[UO_2(H_2O)_5]^{2+}$, $2(ClO_4^-)$, $2(H_3CCN)$, H_2O, ref-code FUVFOR, see: Rogers, R. D.; Kurihara, L. K.; Benning, M. M. *J. Inclusion Phenom. Macrocyclic Chem.* **1987**, *5*, 645. (c) For $C_{12}H_{24}O_6$,$[UO_2(H_2O)_5]^{2+}$, $2(F_3CSO_3^-)$, ref-code LEYYOD, see: Deshayes, L.; Keller, N.; Lance, M.; Nierlich, M.; Vigner, J.-D. *Acta Crystallogr., Sect. C: Cryst. Struct. Commun.* **1994**, *50*, 1541. Note that the average distances may hide important disparities. For instance, in solid-state structures involving the $[UO_2(OH_2)_5]^{2+}$ moiety, r(U═O) ranges from 1.66 to 1.90 Å, and r(U−OH_2), from 2.40 to 2.46 Å. In a given structure, the U−OH_2 distances can differ by up to 0.2 Å (ref 37a).

Table 1. Selected Geometrical Parameters (Bond Distances in Å)[a] and Relative Energies of **1a** and **1b** Relative to **1c** (kcal/mol), Obtained with the BLYP Functional

compound/parameter		LANL	ZORA	CP-opt	CPMD	ZORA(*aq*)	CPMD(*aq*)
1a	r(U═O)	1.80	1.79	1.78	1.78(1)	1.81	1.81(3)
	r(U−O$^{1-5}$)	2.53	2.53	2.50	2.54(8)	2.48[b]	2.48(10)
	E_{rel}	4.6	4.7	3.9	2.2[c]	5.8	−8.7[c]
1b	r(U═O)	1.80	1.79	1.78	*d*	1.81	*d*
	r(U−O^{1})	2.55	2.54	2.54		2.48[e]	
	r(U−O^{2,5})	2.52	2.53	2.49		2.49[e]	
	r(U−O^{3,4})	2.50	2.51	2.47		2.49[e]	
	E_{rel}	2.0	4.5	3.5		5.6[e]	
1c	r(U═O)	1.80	1.79	1.78	1.79(4)	1.81	1.81(3)
	r(U−O^{1})	2.37	2.36	2.36	2.39(4)	2.34	2.39(8)
	r(U−O^{2,4})	2.48	2.47	2.45	2.46(5)	2.41	2.39(8)
	r(U−O^{3})	2.49	2.48	2.46	2.47(5)	2.42	2.39(8)
	r(H···OH$_2$)	1.43	1.44	1.48	1.61(12)	1.52	1.72(17)

[a] Averaged values, where appropriate; in parentheses, standard deviations over the CPMD trajectories. [b] During the ZORA(*aq*) optimization, the hydrogen atoms of the H_2O molecules bend slightly so that the overall symmetry is reduced from approximate D_{5h} to C_{2v}. [c] Free energy (see text). [d] Indistinguishable from **1a**. [e] During the ZORA(*aq*) optimization, **1b** afforded a structure very close to that of **1a**.

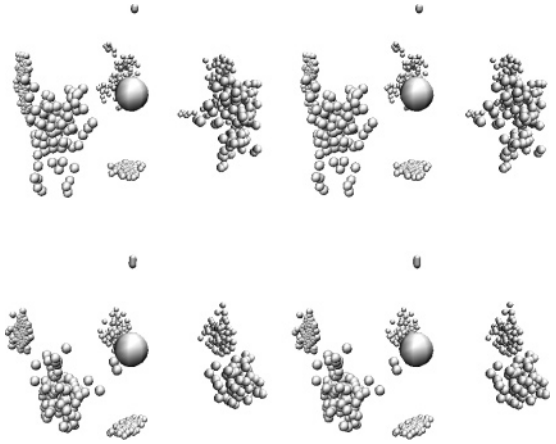

Figure 1. Overlay of snapshots from CPMD simulations of $[UO_2(OH_2)_5]^{2+}$ (stereoviews, H atoms omitted for clarity): (top) gas phase, (bottom) aqueous solution (solvent molecules omitted). The O═U═O^{2+} ion is aligned "vertically". Note the position of the five equatorial water is much more "smeared out" in the gas phase (top) than in water (bottom).

Table 1 do not refer to the respective PESs but to Helmholtz free energies obtained by pointwise thermodynamic integration (PTI)[31] of the mean constraint force $\langle f \rangle$ along a predefined reaction coordinate via

$$\Delta A_{a\rightarrow b} = -\int_a^b \langle f(r) \rangle \, dr \qquad (1)$$

where one U−O(H_2) distance was chosen as reaction coordinate r. These energies thus include entropic contributions missing in the other E_{rel} data. Nevertheless, the relative stability of **1c** over **1a**/**1b** in the gas phase has been found to be qualitatively the same on the free and the potential energy surfaces (compare CP-opt and CPMD energies for **1a** in Table 1). In water, in contrast, the PTI procedure has afforded reversal of this relative stability, placing the hydrated four-coordinate form, $[UO_2(OH_2)_4]^{2+}$, considerably above the hydrated five-coordinate species **1a** (compare CPMD and CPMD(*aq*) energies in Table 1). Isomer **1c** with but one water molecule attached to the $[UO_2(OH_2)_4]^{2+}$ core is certainly not a good model for the fully hydrated four-coordinate form in water. It is thus not surprising that the relative energy of **1a**/**1b** vs **1c** is not reversed with the COSMO continuum model (compare ZORA and ZORA(*aq*) energies in Table 1). Interestingly, the dissociation energy for the simple water detachment reaction

$$[UO_2(OH_2)_5]^{2+} \rightarrow [UO_2(OH_2)_4]^{2+} + H_2O, \qquad \Delta E_{diss} \qquad (2)$$

drops from ΔE_{diss} = 20.5 kcal/mol in the gas phase (ZORA level, cf. 20.8 kcal/mol at CP-opt[11a]) to 2.2 kcal/mol in the continuum. From these simple continuum results, however, no clear-cut conclusion regarding the relative stability of four- and five-coordinated uranyl in water can be drawn, and more sophisticated cluster models including a complete second solvation shell should be employed. Using such models with explicit inclusion of this shell, pentacoordination of uranyl is clearly favored in water.[32d,f,38]

What is the structure of this solvation shell? In the CPMD simulation of $[UO_2(OH_2)_5]^{2+}$ in water, the five equatorial water ligands act as H-bond donors to two solvent molecules each. During the total (unconstrained) simulation time of 4.5 ps, these 10 water molecules are tightly bound to the $[UO_2(OH_2)_5]^{2+}$ core and do not exchange with water molecules from the bulk.[39] The same was found in two other, independent trajectories of the same system during ca. 3 ps each.[40] In the U−O radial distribution function (RDF) displayed in Figure 2, these 10 water molecules are the principal components of the broad peak around ca. 4.6 Å. When integrated up to the next shallow minimum at r = 5.45 Å, the total number of O atoms in this sphere is 14.5 (excluding the seven O atoms from the complex itself). There are thus additional water molecules in this region of space, which are linked via extended H-bond chains to the water ligands of the complex. A very similar RDF has been reported in a recent classical MD study.[32g]

(38) For earlier quantum-chemical studies of metal hydrates with second hydration shells, for instance, see: (a) Martinez, J. M.; Pappalardo, R. R.; Marcos, E. S. *J. Phys. Chem. A* **1997**, *101*, 444−4448. (b) Pavlov, M.; Siegbahn, P. E. M.; Sandström, M. *J. Phys. Chem. A* **1998**, *102*, 219−228.

(39) For many hydrates of the first transition row, present-day functionals (including BLYP) are indicated to underestimate the length (and, possibly, overestimate the strength) of H···O hydrogen bonds to water molecules from the second hydration sphere; see: Rotzinger, F. R. *J. Phys. Chem. B* **2005**, *109*, 1510−1527; this potential shortcoming could affect the lifetime of the water molecules in the second hydration sphere during the simulation.

(40) These simulations were started from constrained CPMD runs performed at the beginning and at the end of the forward and reverse paths, respectively, connecting **1** to a transient hexahydrate (cf. ref 11b), lifting the constraint (which involved the difference between two U−O distances and which had given rise to very small mean constraint forces at both points), and running for a total of 3 and 3.3 ps. The resulting trajectories can be considered as uncorrelated to that from ref 11a. For the RDFs shown in Figures 2 and 3, the last 3.5 ps from the latter trajectory and the last 2.5 ps from each of the new ones were employed.

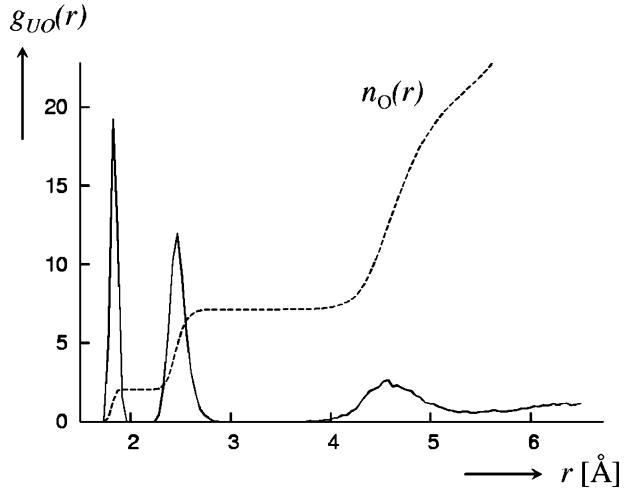

Figure 2. U−O radial distribution function $g(r)$ in a CPMD simulation of $[UO_2(OH_2)_5]^{2+}$ in water (solid line) and integral affording the number of O atoms in a sphere with radius r around U (dashed).

It is in the same region of the RDF where water molecules from the bulk acting as H-bond donors to the terminal oxo ligands of the uranyl moiety would show up. Despite the high positive charge of the UO_2^{2+} fragment, the terminal O atoms can be basic enough to form interactions in the solid state with electrophiles such as metal ions,[41] or with strong Lewis acids,[42] and can act as H-bond acceptors.[43] The latter property has been exploited in the design of "stereognostic" chelators for the uranyl ion.[44]

How many, if any, U═O···H_2O contacts are formed in aqueous uranyl hydrate? In the RDF between the terminal oxo atoms and the O atoms from the bulk solvent (shown on the bottom of Figure 3), a minimum O···O distance of 2.6 Å is apparent, and a shallow maximum is noticeable at $r = 3.1$ Å, a typical threshold for O···H—O hydrogen bonding. On average just one water molecule from the solvent is approaching the terminal oxo ligand closer than this limit, as evidenced from the integral $n_O(r)$ over the RDF (dashed line). Closer inspection of the orientation of these potential H-bond donors reveals that only ca. 40% of these have the OH bond vector oriented toward the oxo atom (i.e., with an O···H—O angle larger than 140°). A similarly low value is apparent from the $g_{OH}(r)$ RDF and its integral, $n_H(r)$, displayed on top of Figure 3 (i.e., involving uranyl oxo ligands and H atoms from the bulk solvent). Really close U═O···H_2O contacts with O···H distances below 2 Å are scarce and fleeting and are rarely maintained for longer than a few hundred femtoseconds. This short residence time is illustrated in Figure 4, a plot of the O···H distances between one oxo atom and those water molecules that are classified, according to the aforementioned geometrical criteria, as H-bonded during the last 2.6 ps of simulation. In short, the overall

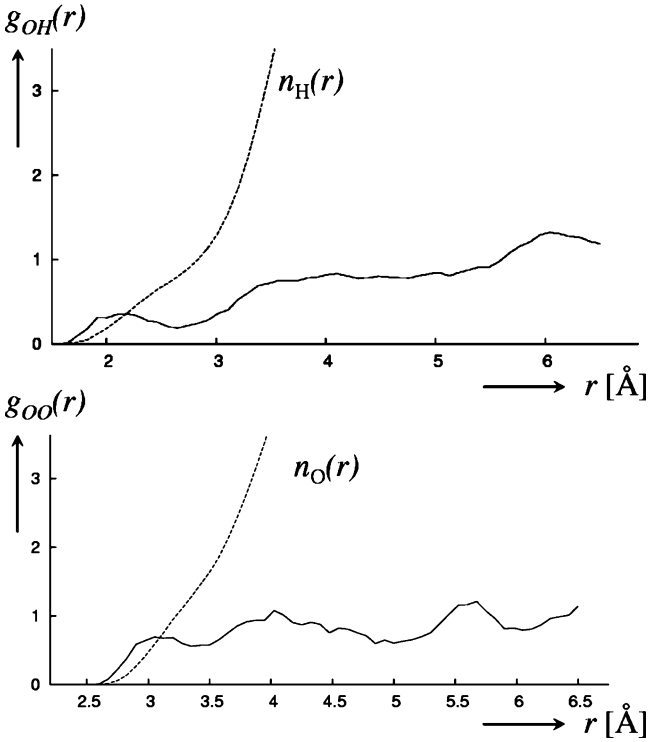

Figure 3. Partial radial distribution functions $g(r)$ between the terminal uranyl oxo atoms of $[UO_2(OH_2)_5]^{2+}$ and H (top) or O atoms from the bulk (bottom); dashed lines: integral affording the number of solvent H or O atoms in a sphere with radius r around (U═)O.

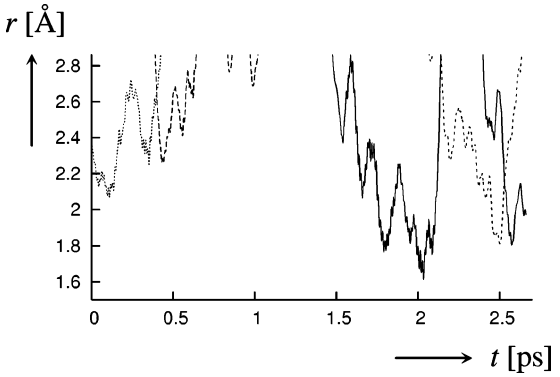

Figure 4. Selected (U═)O···H distances between terminal uranyl oxo and solvent H atoms during CPMD simulation of aqueous $[UO_2(OH_2)_5]^{2+}$.

behavior of the terminal uranyl oxo atoms is rather hydrophobic, even though specific, but very short-lived U═O···H_2O contacts can occur.[45]

How does the electron distribution in uranyl hydrate change upon solvation? A rough impression is provided by the Mulliken atomic charges collected in Table 2. The shortcomings of Mulliken population analysis (MPA) and, in particular, the basis-set dependence of the resulting atomic charges are well recognized.[46] Relative trends, however, should be described quite faithfully. It turns out that, at any given level, the MPA charges for $[UO_2(OH_2)_4]^{2+}$, **1a**, and **1b** are each very similar, varying at most by a few tenths of a charge unit. Thus, only the data for one representative complex, **1a**, are given in Table 2.

(41) For example, see: (a) Na^+: Barnhart, D. M.; Burns, C. J.; Sauer, N. N.; Watkin, J. G. *Inorg. Chem.* **1995**, *34*, 4079−4084. (b) Li^+: Danis, J. A.; Lin, M. R.; Scott, B. L.; Eichhorn, B. W.; Runde, W. H. *Inorg. Chem.* **2001**, *40*, 3389−3394.

(42) For example, see: $B(C_6F_5)_3$: Sarsfield, M. J.; Helliwell, M. *J. Am. Chem. Soc.* **2004**, *126*, 1036−1037.

(43) For instance toward water or ammonia ligands bonded to other metals, such as in $[Co(NH_3)_6]^{3+}$: Clark, D. L.; Conradson, S. D.; Donohoe, R. J.; Keogh, D. W.; Morris, D. E.; Palmer, P. D.; Rogers, R. D.; Tait, C. D. *Inorg. Chem.* **1999**, *38*, 1450−1455.

(44) Franczyk, T. S.; Czerwinski, K. R.; Raymond, K. N. *J. Am. Chem. Soc.* **1992**, *114*, 8138−8146.

(45) In their recent classical MD simulations based on a CASPT2-derived force field, Roos et al. do not observe hydrogen bonding between water and the uranyl oxygens, cf. ref 32g.

(46) Wiberg, K. B.; Rablen, P. R. *J. Comput. Chem.* **1993**, *14*, 1504−1518.

Table 2. Selected Mulliken Charges for **1a** at Various Levels (in Parentheses, NPA Charges)

level	U	O(=U)	$[UO_2]^a$	$O(H_2)$
LANL	1.46	−0.25	0.96	−0.55
(LANL, NPA)	(3.21)	(−0.81)	(1.59)	(−1.02)
ZORA	2.43	−0.51	1.40	−0.54
ZORA(*aq*)	2.57	−0.61	1.35	−0.58
CP-opt	2.23	−0.41	1.41	−0.89
CPMD(*aq*)	2.28(1)	−0.51(1)	1.26(1)	−0.88(0)

[a] Sum for UO_2 moiety. [b] Standard deviation over 10 snaphots from the last 2.5 ps in parentheses.

As expected, the MPA results for the pristine complex can be quite dependent on the particular level; for instance, the calculated charge on U can vary by almost a total charge unit (compare LANL and ZORA data in Table 2). Interestingly, the ZORA and CP-opt results are quite consistent with each other as far as the uranyl moiety is concerned. With both approaches, a small charge transfer onto this moiety, as well as a small increase in its polarity, is found in the solvent, where the charges on the metal and on the uranyl O atoms are both increased in absolute terms by ca. 0.05−0.1*e* (compare ZORA vs ZORA(*aq*) and CP-opt vs CPMD data in Table 2).

2. $UO_2(NO_3)_2(OH_2)_2$. We now turn to uranyl dinitrate **2**, which has been characterized in numerous solids as a trans isomer with two bidentate nitrate ligands (**2a**, Chart 3).[12] In Table 3 salient geometrical parameters are collected for this molecule, as obtained with the different theoretical approaches. The CP calculations were performed in a rectangular box large enough to accommodate this rather oblate molecule (16 × 13 × 16 Å^3).

As in the case of **1**, the various BLYP results are in good mutual accord (compare, e.g., LANL, ZORA, and CP-opt entries), as is the effect of solvation (compare, e.g., CPMD vs CPMD(*aq*) and ZORA vs ZORA(*aq*)). Interestingly, opposing solvent effects are apparent for the distances to water and nitrate: while the former are shortened in water, as for uranyl hydrate discussed above, the latter are significantly elongated upon solvation. The strong Coulomb attraction between the uranyl dication and the nitrate anions that is present in the pristine complex in the gas phase is thus significantly reduced by the presence of a polar solvent. In water, the anionic ligand can form specific interactions not only with the cation but also with the solvent. These interactions are apparent in partial RDFs involving O atoms from the nitrate groups and H or O atoms from the bulk water, as illustrated in Figure 5 (the larger noise in this figure compared to that in Figures 2 and 3 is due to the poorer statistics related to the rather short total simulation time of ca. 2 ps for **2a**, after 1 ps taken as equilibration, as opposed to ca. 8.5 ps for **1**[40]). In particular for the terminal nitrate O atoms protruding into the solution, a broad peak is apparent in $g_{OO}(r)$ between ca. 3 and 4 Å (solid line in the bottom of Figure 5). No such peak is visible for the nitrate O atoms coordinated to U (dashed line in Figure 5), where, however, $g_{OO}(r)$ has all but attained its isotropic average value of 1 in this region. Since a large fraction of the volume around these O atoms is occupied by the complex (where no water molecules from the solvent can be found), much smaller *g* values would be expected in the complete absence of near-order. Integration of the RDFs up to $r = 3.5$ Å affords a total number of $n_O(r) = 6.9$ water molecules around all O atoms of one nitrate ligand (half of which are associated with the terminal O atom of the latter). According to the integral over the corresponding $g_{OH}(r)$ RDF (top of Figure 5), about half of those water molecules, in total 3.3 per nitrate, have their H atoms located within hydrogen-bonding distance, that is, within ca. 2.7 Å of any nitrate O atom.

The nitrate groups are thus well solvated in water, and the bonding to the metal is weakened. In contrast to uranyl hydrate **1a**, where solvation reinforced bonding and stiffened the orientation of the equatorial ligands (cf. Figure 1), the nitrate moieties in **2a** become quite flexible in water, where also notable out-of-plane motions persist. At no point in these unconstrained simulations, however, was a clear reduction in hapticity observed.

To get more information concerning the actual preference of the chelating binding mode, we performed static optimizations for η^1-bonded nitrate complexes in the gas phase, as well as constrained CPMD simulations enforcing such a coordination, followed by PTI. It turned out that, in the gas phase, at least four minima of **2a** exist in which one nitrate moiety is coordinated in η^1-fashion. Two are depicted in Chart 3, namely **2b**, where one intramolecular H-bridge to a water ligand is formed, and **2c**, with two such contacts to both water ligands. In **2b** and, even more so, in **2c**, the η^1-coordinated nitrate is strongly bent out of the equatorial plane (defined by the η^2-nitrate, the metal, and the two water O atoms) by 48.1° in **2c** (LANL level).[47] At the LANL level, **2b** and **2c** are both 6.6 kcal/mol less stable than **2a** in the gas phase. Similar numbers for **2b** and **2c** are obtained with ZORA (6.4 and 8.3 kcal/mol, respectively) or CP-opt (6.2 kcal/mol). There are also two other minima closely related to **2b** and **2c** with different relative orientations of those OH bonds that are not involved in H-bonding ("up" or "down" with respect to the equatorial plane). Both pairs of minima are virtually isoenergetic, and from the CPMD results in the gas phase (see below) it appears that interconversion between them is very facile. The transition state between **2a** and **2b**, **TS2ab** (depicted in Figure 6), is 9.4 kcal/mol higher than the reactant η^2-minimum (LANL level, ZORA: 8.4 kcal/mol).

To keep the CPU-expensive constrained CPMD simulations tractable, we employed a smaller, cubic box with a length of 13 Å, where we aligned the molecule with its longest axis along the diagonal of the cube. In this setup there is enough space between the replicated periodic images. However, the molecules are more hindered in their rotational mobility in this box, as they could bump into each other when rotating toward one of the lattice vectors. Indeed, geometrical differences between the CPMD(*aq*) simulations in both boxes (with the same density) are noticeable and amount to ca. +0.01, −0.02, and +0.03 Å for the mean U−O(nitrate), U=O, and U−O(H_2) distances, respectively (the sign denoting the change upon going from the larger into the smaller box). Since the stretching potentials for these bonds are relatively flat, however (e.g, the normal thermal fluctuations for these bonds are much larger than these changes; see the standard deviations in Table 3), the energetics should not be affected seriously, and the resulting free energies should be entirely reasonable.

(47) It is also noteworthy that, in the equilibrium structures of pristine **2**, the water ligands are tilted away from the U−O(H_2) axis (e.g., for **2a** the angle between this U−O axis and the plane of one water molecule is 127.8° at the LANL level), whereas predominantly coplanar UOH_2 moieties are found in the CPMD simulations in water (cf. snapshots on the bottom of Figure 7).

Chart 3

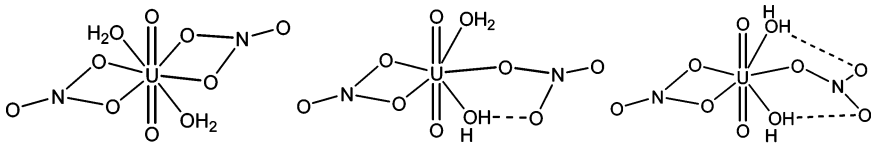

2a **2b** **2c**

Table 3. Selected Geometrical Parameters (Bond Distances in Å)[a] of **2a**, Computed with the BLYP Functional and Observed in the Solid

parameter	LANL	ZORA	CP-opt	CPMD	ZORA(*aq*)	CPMD(*aq*)	X-ray[b]
r(U═O)	1.82	1.81	1.80	1.81(3)	1.82	1.83(5)	1.75
r(U−OH_2)	2.62	2.62	2.59	2.66(17)	2.55	2.43(7)	2.39
r(U−ONO_2)	2.54	2.51	2.49	2.51(8)	2.53	2.59(24)	2.53
r(N−O^t)	1.22	1.22	1.22	1.22(3)	1.23	1.23(2)	1.22
r(N−O(U))	1.31	1.31	1.31	1.32(3)	1.30	1.31(4)	1.27

[a] Averaged values, where appropriate; in parentheses, standard deviations over the CPMD trajectories (for values for the larger box, see Computational Details). [b] From ref 12a (standard deviations quoted between 0.002 and 0.004 Å); the two uranyl-coordinated water ligands form intermolecular contacts to one cocrystallized water molecule and nitrate ion each (with protonated terpyridyl as counterions).

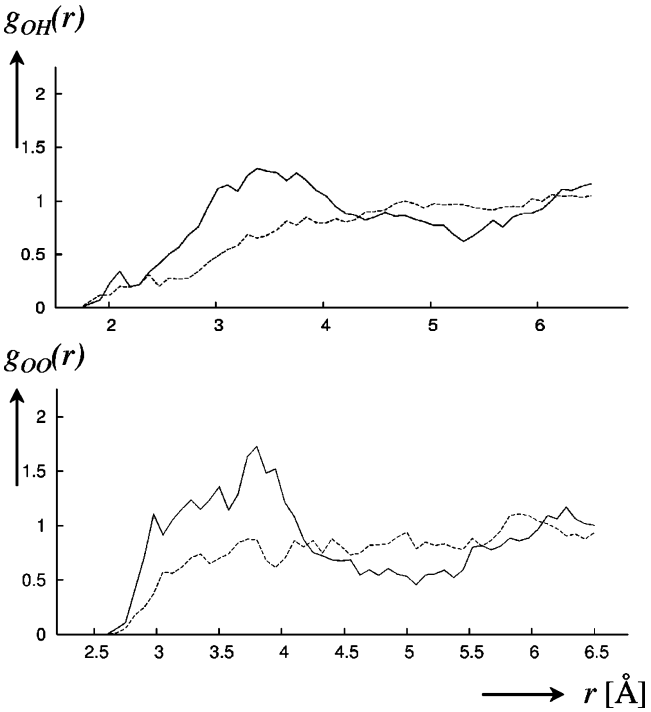

Figure 5. Partial radial distribution functions $g(r)$ between the nitrate O atoms of **2a** and H (top) or O atoms from the bulk (bottom): (solid line) terminal nitrate O atom; (dashed line) uranyl-coordinated nitrate O atoms.

For the PTI technique, we chose the difference Δr between two U−O distances to one nitrate as reaction coordinate for eq 1. Starting from **2a** with a difference of $\Delta r = 0$, we successively increased this value in steps of 0.2 Å and performed constrained MD simulations until the running average of $\langle f \rangle$ was reasonably well converged (typically within 1.5 ps after 0.5 ps of equilibration). The resulting energy profile in the gas phase is depicted in Figure 7 (dashed line).

A minimum on the ΔA surface is obtained for this coordinate at $\Delta r = 1.4$ Å. The structures sampled in that region resemble **2b** with the intramolecular hydrogen bond between the nitrate O atom and one water ligand (cf. the snapshot at the upper right in Figure 7). The molecule is quite flexible in that region, however, and the "free" water ligand, for instance, shows essentially unhindered rotation about the U−O(H_2) bond. Near the end of the simulation for $\Delta r = 1.6$ Å, that is, after the desired

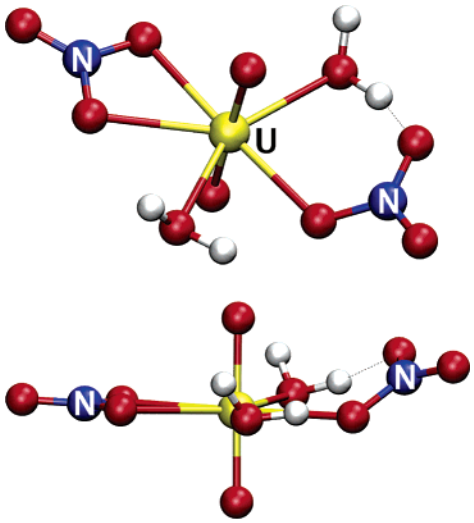

Figure 6. Two views of the transition state **TS2ab** between η^2- and η^1-bonded nitrate in **2**.

η^2-η^1 transition was all but completed, the intramolecular hydrogen bond was broken, and the nitrate group flipped to the other side, forming the same kind of H-bond between the third nitrate O atom (the "dangling" one up until then) and the other water ligand. This rearrangement occurred via transient structures resembling **2c**. On the free energy surface, the minimum corresponding to **2b** is 3.9 kcal/mol above **2a**. This value is comparable to the relative energies on the PES, 6.2 kcal/mol at CP-opt, in particular when allowing for entropy effects. The latter (together with the enthalpic contributions) are indeed indicated to stabilize **2b** relative to **2a**, e.g., by 1.1 kcal/mol for the Gibbs free energies at the LANL level, as obtained from standard thermodynamic corrections using computed harmonic vibrational frequencies. The free-energy barrier between **2a** and **2b** is found at $\Delta r = 0.8$ Å and $\Delta A^{\ddagger} = 5.8$ kcal/mol, again somewhat lower than the corresponding static values on the PES (e.g., 9.2 kcal/mol at LANL, 9.6 kcal/mol for $\Delta G^{\ddagger}$ at that level). It appears, however, that the MD-based PTI approach in general affords the same qualitative description of the η^2-to-η^1 transition that is emerging from the stationary points on the underlying PES and that no serious artifacts are introduced with the chosen parameters and reaction coordinate.

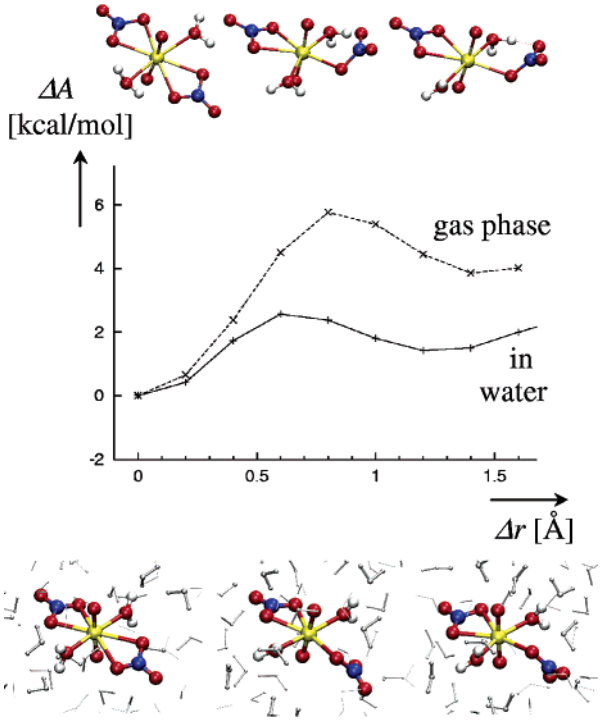

Figure 7. Change in free energy, ΔA, for η^2-to-η^1 transition of one nitrate ligand in $UO_2(NO_3)_2(OH_2)_2$, as obtained from constrained CPMD simulations and thermodynamic integration (reaction coordinate: difference Δr between two U−O(nitrate) distances). Representative snapshots from the respective bidentate, transition-state, and monodentate regions are included for the gas phase (top) and the aqueous solution (bottom).

When the PTI procedure is repeated starting from **2a** in aqueous solution, the computed changes in free energy (solid line in Figure 7) are even smaller than those in the gas phase. Again, a free-energy minimum is apparent, now at $\Delta r = 1.2$ Å and $\Delta A = 1.4$ kcal/mol. Unlike in the gas phase, this minimum does not correspond to an intramolecularly H-bonded complex resembling **2b** or **2c** (see snapshot at the lower right of Figure 7). In water, the two uranyl-bonded water ligands are donating fairly strong hydrogen bonds to the solvent. These H-bonds are persistent on the picosecond time scale (on which, for instance, no exchange between water molecules from this second solvation sphere and those from the bulk is observed), and the uranyl water ligands are not available for interaction with the nitrate. As discussed above, the latter is rather forming intermolecular hydrogen bonds with the solvent.

In the region of the shallow free-energy minimum between $\Delta r = 1.0$ and 1.4 Å the mobility of the η^1-nitrate is visibly enhanced. The O atom that is losing contact to uranium becomes free to leave the equatorial plane, and the η^1-bonded nitrate ligand commences rotational motions about the uranyl-bonded NO bond. With increasing Δr, there is a certain propensity for perpendicular orientation of the η^1-nitrate relative to the equatorial plane (as apparent from the snapshots in the lower right of Figure 7). The computed free-energy barrier is very low, 2.6 kcal/mol (at $\Delta r = 0.6$ Å) relative to **2a**, and lies only 1.2 kcal/mol above the shallow η^1-minimum.

It is possible that, in this region, the PTI-derived ΔA values are associated with a somewhat larger statistical error due to potentially incomplete sampling of the accessible phase space that is increasing as the hapticity of the nitrate is reduced. It is thus not fully clear if the occurrence of the shallow minimum

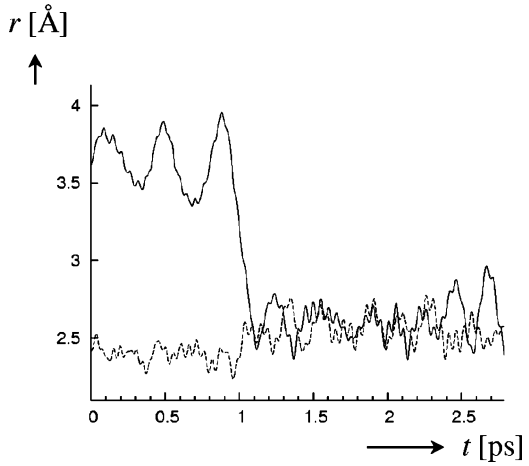

Figure 8. Evolution of the two U−O(nitrate) distances in $UO_2(NO_3)_2(OH_2)_2$, starting with a difference $\Delta r = 1.2$ Å, after release of the constraint.

at $\Delta r = 1.2$ Å is real or if it could be an artifact of the PTI procedure applied to what would rather be best described as a shallow plateau. To test this possibility, we continued the simulation at $\Delta r = 1.2$ Å from the last point, releasing the constraint. As is illustrated in Figure 8, a plot of the two salient U−O(nitrate) distances, the η^1-like configuration is stable for ca. 1 ps before it collapses to the η^2-minimum. During that time it can undergo three bending vibrations about the U−O−N angle, visible in Figure 8 from the oscillations in the distance to the initially nonbonded O atom (solid line). Thus, there indeed appears to be a local minimum in this region (or a set of closely spaced ones) deep enough to be stable for a short time if populated. A shallow but rugged plateau would also be consistent with this result. Note that the actual η^1-to-η^2 transition happens very quickly, within ca. 200 fs (see the sharp drop of the solid line in Figure 8). Note also that the η^2-bonded nitrate is very flexible and that the bonded U−O distances can reach instantaneous values of up to ca. 3 Å (see peaks in Figure 8 around 2.5 ps). The same is found in the unconstrained CPMD simulations starting from **2a** in water.

Irrespective of the characterization of the η^1-bonded region as a shallow minimum or as a shallow plateau, what is clear from the PTI results is that the transition from η^2- to η^1-bonded nitrate is significantly facilitated upon solvation. The computed free energy of activation for this process is more than halved, from 5.8 kcal/mol in the gas phase to 2.6 kcal/mol in water. This apparent weakening of the binding to one arm of the chelate is fully consistent with the U−O(nitrate) bond distances discussed above, which are found to increase upon hydration. Solvation effects on geometrical parameters and binding energies are thus opposite for the nitrate ion in **2** and the neutral water ligand in **1**. For the latter, hydration reinforces bonding, as reflected in shortened U−O(H_2) distances and a larger dissociation energy for one ligand in water.

3. $UO_2(NO_3)_2$(tmma). We now turn to complex **3**, calling special attention to the preference of the η^2- vs the η^1-binding mode of the chelating diamide ligand. This section is organized as follows: first, the results from static gas-phase optimizations are discussed in their context with closely related complexes involving other anionic and chelating ligands. This part will both motivate the particular choice of **3** as a target in this study and serve as further validation of the CP-setup with the uranium pseudopotential, as far as relative energies of isomeric com-

Chart 4

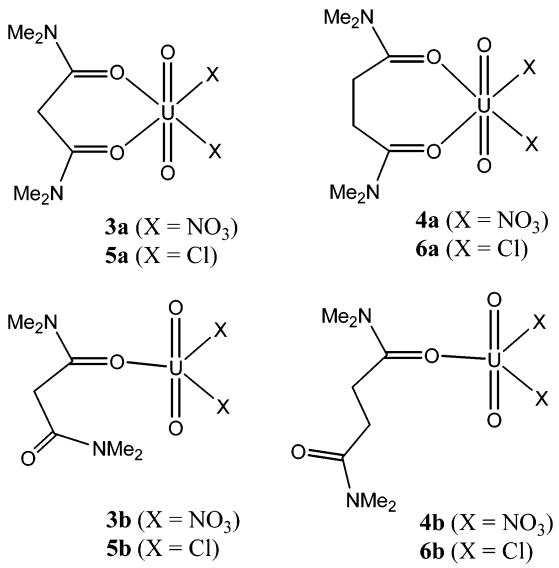

Table 4. Relative Energy $\Delta E_{mono/bi}$ (= $E_{mono} - E_{bi}$, in kcal/mol) of Monodentate (**b**) vs Bidentate (**a**) Uranyl Complexes; Positive Values Indicate that the Latter Are More Stable

	complex			
level	**3**	**4**	**5**	**6**
HF/LANL[a,b]	0.7 (0.0)	1.3 (0.2)	7.5 (7.1)	10.0 (7.8)
MP2/LANL[a,c]	1.5	2.0	9.0	12.3
B3LYP/LANL[a]	1.6	1.9	6.0	8.8
BLYP/ZORA	1.4	3.5	5.6	9.0
BLYP/CP-opt	0.4	1.3	5.8	10.4
BLYP/ZORA(*aq*)	10.5	10.8	1.9	4.7

[a] From ref 6b. [b] In parentheses: $\Delta G°$ values. [c] Single points on B3LYP/LANL geometries

plexes are concerned. Finally, CPMD results of η^2- and η^1-variants of **3** in vacuo and in water are evaluated.

3.1. Static Calculations: The preference of η^2- over η^1-binding of chelating diamide ligands to uranyl has previously been studied at HF and B3LYP levels for a small set of complexes in the gas phase (**3**−**6**, Chart 4).[6b] Depending on the size of the anionic ligands and on the ring size of the diamide chelates, the monodentate isomers were found between ca. 1−10 kcal/mol above the corresponding bidentate ground states. We have now reoptimized these minima at the BLYP level and checked that the salient geometrical parameters (see below for a specific example), as well as the resulting energy differences $\Delta E_{mono/bi}$ between η^1- and η^2-forms (collected in Table 4), are consistent with these reference data. The CP calculations were performed in a rectangular box large enough to accommodate the largest of these molecules, **4b** with the extended chain of the monodentate ligand (19 × 16 × 12 Å^3).

Again, the CP-opt results are qualitatively consistent with the other DFT methods using the same functional, which can be taken as further evidence for the reliability of the uranium pseudoptential and its transferability and applicability to a variety of uranyl(VI) complexes (see also the geometrical parameters collected in Table 5 below, as well as in Tables S1 and S2 of the Supporting Information). Likewise, the BLYP results are in line with the previous B3LYP data, as well with the HF and MP2 energies. All methods agree that the energetic separation between mono- and bidentate coordination decreases on going

Table 5. Selected Geometrical Parameters (Bond Distances in Å) of **3a**, Computed with the BLYP Functional and Observed in the Solid

parameter[a]	ZORA	CP-opt	CPMD[b]	ZORA(*aq*)	CPMD(*aq*)[b]	X-ray[c]
(U═O)	1.82	1.81	1.81(3)	1.83	1.83(4)	1.78
r(U−O(C))	2.53	2.53	2.57(11)	2.38	2.38(7)	2.41
r(U−O(N))	2.52	2.50	2.53(11)	2.59	2.59(13)	2.51
r(C═O)	1.25	1.25	1.26(3)	1.28	1.28(3)	1.17
r(N−O(U))	1.31	1.31	1.31(3)	1.30	1.30(4)	1.26
r(N−O^t)	1.23	1.22	1.23(2)	1.24	1.24(3)	1.20

[a] Average values for nonequivalent distances, if applicable. [b] In parentheses, standard deviation. [c] From ref 13 (standard deviations quoted as 0.005−0.02 Å).

Chart 5

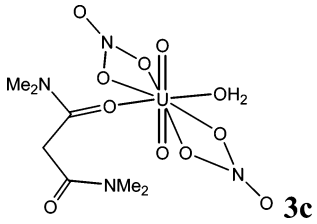

from chloro to nitrate and from seven- to six-membered chelate rings. For $UO_2(NO_3)_2$(tmma) (**3**) both coordination modes are almost isoenergetic. In solution, the monodentate forms should be stabilized even further, since the binding energy of an additional water molecule from the solvent to the uranyl moiety in these forms is sizable,[48] possibly outweighing the entropic penalty for such an associative process. With these observations in mind, we performed CPMD simulations of aqueous solutions of complex **3** in both hapticities of the diamide ligand.

3.2. CPMD Calculations: For quantitative estimates of the relative stability it would be desirable to apply the PTI technique to a suitable reaction coordinate connecting both coordination modes. It is very difficult, however, to devise a small yet unbiased set of geometrical parameters for this purpose. Moreover, the larger box size compared to that employed for **1** and **2** would render the necessary large number of constrained MD runs very CPU-expensive. We thus performed four unconstrained CPMD simulations in vacuo and in water each for **3a** and **3b**, hoping that we could observe a spontaneous transition in one or the other direction. Since the CPMD simulations of the aqueous solution started from well-equilibrated classical MD runs, in which **3b** rapidly captured a water molecule from the solvent, the simulations for the monodentate form describes actually the monohydrated adduct **3c** (Chart 5).

The CPMD simulations were followed for a total of 10 ps for gaseous **3a** and 4 ps each for aqueous **3a**, gaseous **3b**, and aqueous **3c**. No rearrangements of the tmma ligand were observed in any of these cases. This ligand is quite flexible in the gas phase, where instantaneous elongations of individual U−O(carbonyl) distances up to ca. 3 Å occur frequently (see the corresponding plot for **3a** in Figure 9). In some of these structures, the transition to η^1-bonded **3b** appeared to be noticeably advanced, as judged from a distinct bending of the distant carbonyl group out of the equatorial uranyl plane. This can be seen in Figure 10 where the O═C···C═O angle of the η^2-bonded **3a** reaches some values close to those observed with **3b**.

(48) For example, the binding energies for the reaction **3b** + H_2O → **3c** are −15.6 and −10.3 kcal/mol at the BSSE-corrected HF/LANL (ref 6b) and BLYP/ZORA levels, respectively.

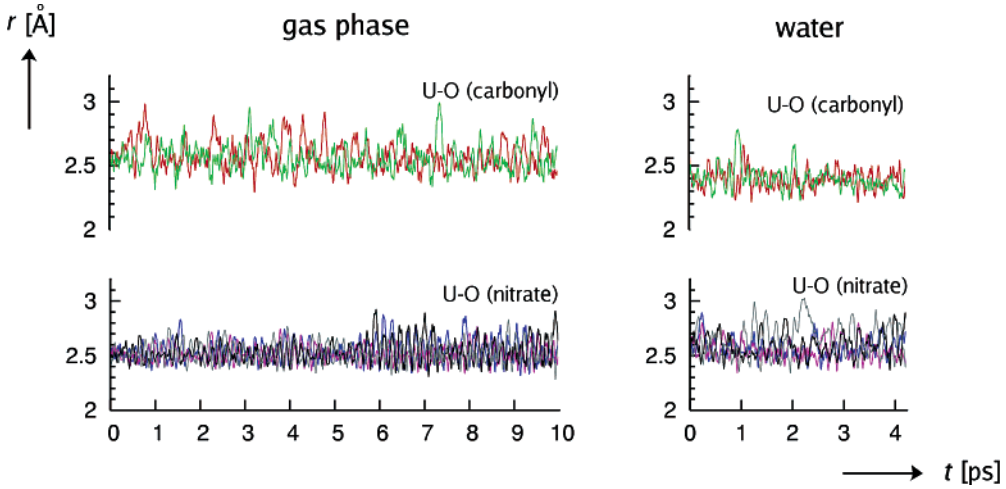

Figure 9. Evolution of U−O(carbonyl) and U−O(nitrate) bond distances in a CPMD simulation of **3a** in the gas phase (left) and in water (right).

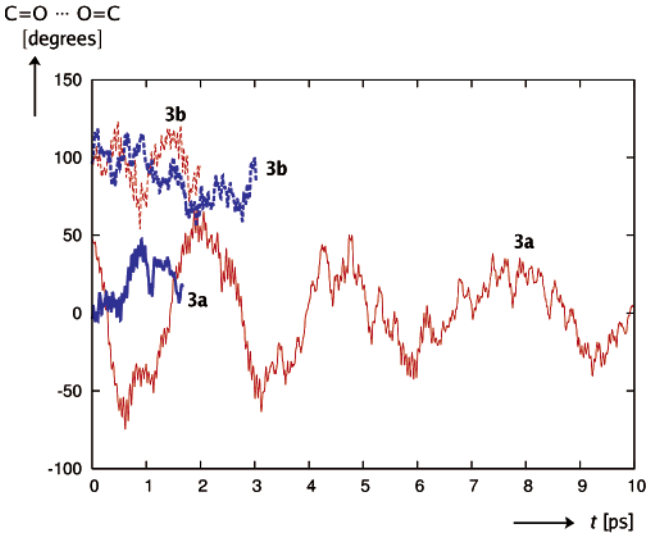

Figure 10. Evolution of the O═C···C═O dihedral angle in CPMD simulations in the gas phase (thin red lines) and in water (dark blue lines), starting from η^1-bonded **3b** (broken lines) or η^2-bonded **3a** (solid lines).

In the simulation of **3a** in water, the diamide is somewhat more strongly bound to uranyl than in the gas phase, as apparent from the U−O(carbonyl) distances, which show a shorter mean value and smaller amplitudes in solution than those for the pristine complex (compare CPMD and CPMD(*aq*) values in Table 5). In contrast, the bonding to the nitrate ligands is weakened in the solvent, as evidenced by increased mean U−O(nitrate) distances and standard deviations of the latter (Table 5). Interestingly, the same trends are apparent from the static optimizations in the continuum (compare ZORA and ZORA(*aq*) entries in Table 4). These findings are fully in line with the situation for **1** and **2**: hydration reinforces bonding between uranyl and neutral ligands such as water or the diamide but weakens the interaction with the anionic ligand, nitrate.[49]

We also performed a CPMD simulation for aqueous **3a** at an elevated temperature, 350 K,[50] in order to check if this increase in kinetic energy would promote a complete detachment of one of the carbonyl arms from the metal. However, no such transition happened within 2 ps (the U−O(C) distances and standard deviations remained the same as those obtained at 300 K). Apparently, this process is significantly activated so that much longer unconstrained MD runs would be necessary to overcome the barrier.

Finally, we performed a CPMD simulation for the monodentate form **3c** in water. Rearrangement to the bidentate isomer **3a** would require some larger reorientations in the coordination sphere. Besides coordination of the pendant chelate arm, the two nitrates would have to approach each other from the mutual trans to a cis orientation, with concomitant expulsion of the water ligand. As expected, nothing of this sort happens within the short simulation time of ca. 4 ps. Interestingly, however, during this simulation one nitrate changes from η^2- to η^1-coordination. This transition is monitored in Figure 11 (left), the time evolution of the salient U−O(nitrate) distance (dashed line). The cleavage of this bond is paralleled by a noticeable approach of the pendant carbonyl O atom toward uranium (solid line in Figure 11). It is conceivable that the reduction of hapticity of the nitrate ligand creates enough space for the second amide moiety to coordinate to the metal eventually, without expulsion of the water ligand. In any case it is noteworthy that, as the pendant carbonyl approaches, it is not the nitrate next to it that changes to η^1-coordination but the nitrate in trans position (see the snapshot on the right-hand side of Figure 11).

Only limited conclusions can be drawn from such a singular event (hapticity change), which may be coupled to the instantaneous structure of the surrounding solvent, and much longer simulation times would be necessary for a statistically significant statement. Nonetheless, this finding points to the possibility that the speciation of diamide/nitrate complexes in water can be more complicated than hitherto assumed. In particular, the involve-

(49) This differential solvation effect for complexes involving neutral or anionic ligands arguably arises from a balance between cation−anion, ion−dipole, and dipole−dipole interactions in the dynamic ensemble. Even though the underlying electrostatics are usually modeled quite well with present-day density functionals (which also tend to afford reasonably accurate dipole moments and polarizabilities, cf. Koch, W.; Holthausen, M. C. *A Chemist's Guide to Density Functional Theory*; Wiley-VCH: Weinheim, 2000), such a delicate balance may be difficult to describe, and quantitative inaccuracies might add up to a qualitative change of the overall picture. In context with the types of interactions studied here, however, we note that the solvent-induced bond contraction in metal-aquo complexes (cf. ref 33) is also found with DFT methods (e.g., ref 38b); likewise, the elongation of cation−anion distances in simple contact ion pairs such as alkali-metal or silver halides upon hydration (i.e., the onset of dissociation in water) is also well described with DFT (e.g., Godinho, S. S. M. C.; Cabral do Couto, P.; Costa Cabral, B. J. *J. Chem. Phys.* **2005**, *122*, 044316). Thus, we are confident that our results are qualitatively correct and are not artifacts of the adopted DFT approach.

(50) Effected via restart of the equilibrated 300 K simulation and instantaneous heatup.

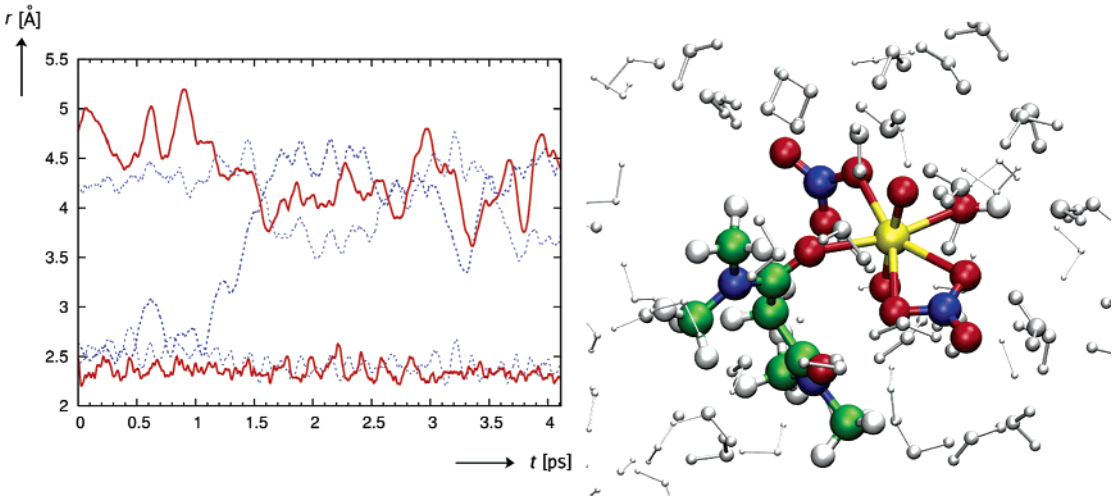

Figure 11. (Left) Evolution of the U−O distances of the salient nitrate's three oxygens (blue dashed lines) and two carbonyl's oxygens (red solid lines) in a CPMD simulation of **3c** in water; (right) snapshot from the end of the simulation showing the η^1-coordinated nitrate in the upper left section.

ment of η^1-bonded nitrate ligands should be taken into consideration. Population of such species, which are potentially more hydrophilic than η^2-bonded ones (cf. the better hydration of terminal over U-coordinated O atoms apparent from Figure 5), could have a noticeable impact on the extraction properties with organic solvents.

As in the constrained MD of **2a** in water (see preceding chapter), the η^1-nitrate in **3c** is quite mobile and can readily rotate about the U−O(nitrate) axis, affording instantaneous structures where the NO_3 plane is aligned parallel with the uranyl axis (see snapshot in Figure 11). That it is one nitrate O atom and not the water ligand that detaches from the metal implies that the activation barrier for the former process is noticeably lower than that for the latter. This ordering would be entirely compatible with the corresponding dissociation energies and barriers for aqueous **2a** and **1a** discussed above: The PTI-derived free energy of activation for formation of the η^1-nitrate in **2a** is 2.6 kcal/mol, much lower than that for water dissociation from **1a**, 10.8 kcal/mol.[11a] Seeing that no nitrate rearrangement was observed in the unconstrained MD simulation of **2a**, the corresponding barrier in **3c** may actually be even smaller than 2.6 kcal/mol.

Even if coordination or detachment of one diamide chelate arm had occurred in these simulations, no quantitative information as to the relative ordering of mono- and bidentate forms would have been obtained. Interestingly, the COSMO continuum model predicts a clear preference for bidentate vs monodentate forms: for instance, the energetic separation between **3a** and **3b** increases from $\Delta E_{\text{mono/bi}} = 1.4$ kcal/mol to 10.5 kcal/mol on going from the ZORA to the ZORA(*aq*) level. Likewise, the binding energy in the reaction

$$\mathbf{3a} + H_2O \rightarrow \mathbf{3c} \qquad (3)$$

changes from −8.9 kcal/mol in the gas phase (ZORA level) to +3.7 kcal/mol in the continuum (ZORA(*aq*) level).[51] Again, the bidentate form **3a** is preferred "in water", which points to the importance of solvation for the chelate effect.

(51) In the COSMO model, it is the screening term that dominates the changes with respect to the gas phase; the dispersion/cavitation term contributes less than 1.5 kcal/mol to the energy differences discussed.

Conclusions

We have studied structures and dynamics of three prototypical uranyl complexes in the gas phase and in aqueous solution, employing a variety of DFT-based approaches together with the BLYP functional. These methods comprise static optimizations in the gas phase and in a polarizable continuum, as well as CPMD simulations of the actual solution. As far as optimized parameters and relative energies of stationary points on the potential energy surface in the gas phase are concerned, all methods show good mutual accord with each other, irrespective of computational details such as choice of relativistic treatment, pseudopotentials, or type of basis set. The CPMD method has been applied to uranyl nitrate complexes for the first time, furnishing insights on an atomic level into dynamics and fluxionality on the picosecond time scale of prototypical species involved in uranyl extraction from nuclear waste. It is now possible to compare the results from simple continuum or mixed discrete-continuum models with those from the dynamic ensemble that take solvation explicitly into account and to contrast MD simulations based on classical force fields with those based on a quantum-chemical method.

The most significant finding for the complexes of this study is that the solvent can have a differential effect on the bonding between uranyl and various types of ligands. A solvent-induced bond strengthening is found between the uranyl moiety and neutral ligands such as water and tmma, a chelating diamide. This bond reinforcement on going from the gaseous to the aqueous phase is manifest in a considerable contraction of the corresponding U−O distances (up to 0.2 Å for the water ligand in **2a**) and, for the pentaquo complex **1a**, in a significant increase of the free energy of dissociation for one of the uranyl−water ligands. In keeping with this uranyl−water bond strengthening, the degree of fluxionality of the water ligands in **1a** is much reduced in solution compared to the gas phase, where large-amplitude motions out of the equatorial plane occur.

The bonds between uranyl and the anionic nitrate ligand, on the other hand, are noticeably weakend upon solvation, as reflected in an elongation of the U−O(nitrate) distances and facilitation of an η^1-binding mode over the usual η^2-coordination of this ligand. The latter effect has been studied for **2a** by means of pointwise thermodynamic integration involving constrained

CPMD simulations along a suitable reaction coordinate. The computed free energy of the monodentate species relative to the bidentate minimum drops from 3.9 kcal/mol in the gas phase to 1.4 kcal/mol in water. There is thus a large impact of solvation on this simple chelate effect. For a particular variant of uranyl nitrate with the tmma ligand, **3c**, this solvent-induced promotion of η^1- vs η^2-binding can be so pronounced that it can be observed in unconstrained CPMD simulations within a few picoseconds.

The MD simulations as presented should be applicable to a wide variety of uranyl complexes in order to study their structure, dynamics, and speciation in solution. The latter aspect, in particular, may be ultimately relevant for understanding the molecular basis of uranyl extraction and separation from metal ions and actinide analogues (e.g., PuO_2^{2+}) and, eventually, for optimizing and controlling the corresponding processes.

Acknowledgment. M.B. wishes to thank W. Thiel, the MPI für Kohlenforschung, and the Deutsche Forschungsgemeinschaft for support. A generous allotment of CPU time on an IBM p690 "Regatta" cluster at Rechenzentrum Garching is gratefully acknowledged. R.D. and W.G. thank CNRS-IDRIS, GDR PARIS, and University Louis Pasteur for support.

Supporting Information Available: Coordinates or geometrical parameters for **TS2ab**, **3b**, and **4**−**6** and a complete author list of refs 17 and 21c (3 pages, PDF). This material is available free of charge via the Internet at http://pubs.acs.org.

JA057301Z